JOURNAL OF AGRICULTURAL AND FOOD CHEMISTRY

pubs.acs.org/JAFC Article

Discovery of Novel Terpenoids from the Basidiomycete *Pleurotus ostreatus* through Genome Mining and Coculture Optimization

Guihong Yu,*[,†] Xiaoxuan Ge,[†] Yu Wang,[†] Xuhua Mo, Hao Yu, Lingling Tan, and Song Yang*

Cite This: *J. Agric. Food Chem.* 2023, 71, 11110−11123 Read Online

ACCESS | Metrics & More | Article Recommendations | Supporting Information

ABSTRACT: In our previous work, postredienes A−C, three unusual linear sesterterpenes with high antifungal activities, were isolated from *Pleurotus ostreatus* SY10 when cocultured with *Trametes robiniophila* SY636. However, their titers were low, and exploration of newly biosynthesized trace analogues is required. Herein, genome mining analysis predicted that 17 gene clusters are involved in terpenoid biosynthesis in *P. ostreatus*. Thus, coculture conditions for strains SY10 and SY636 were optimized using a single-factor test and Box−Behnken design. As a result, the titers of postredienes A−C were increased by over 2.5-fold, reaching 1.28 to 8.40 mg/L. Moreover, five new terpenoids, named postredienes D−H (**1**−**5**), were successfully isolated. Compound **1** exhibited activities against the human pathogenic fungi *Candida albicans* and *Cryptococcus neoformans* comparable to those of amphotericin B. Compound **2** represents a novel sesterterpene with a five-membered ring at C-7. The absolute configurations of **1**−**5** were elucidated by making the methoxyphenylacetic acid esters and acetonide derivatives, combined with ECD and NMR calculation. Two potential gene clusters and relevant biosynthetic pathways for **1**−**5** were subsequently proposed based on real-time reverse transcription-quantitative PCR (RT-qPCR) analysis. The current study provides new insights into the research of terpenoid biosynthesis genes in *P. ostreatus* and other basidiomycetes.

KEYWORDS: *Pleurotus ostreatus, genome mining, optimization of coculture conditions, terpenoids, antimicrobial activity*

INTRODUCTION

Terpenoids from basidiomycete fungi were reported to have high structural diversity and abundant biological activities. For example, diterpene pleuromutilin from *Clitophilus scyphoides* (formerly named *Pleurotus passeckerianus*) and sesquiterpenes illudins from *Omphalotus olearius* (formerly named *Clitocybe illudens*) are two types of drug leads. Pleuromutilin exhibits potent antibacterial activities, while illudins demonstrate remarkable antitumor activities.[1,2] *Pleurotus ostreatus*, the second most commonly cultivated mushroom after *Agaricus bisporus* globally, can be easily cultivated, exhibits rapid growth, and possesses a great value in nutrition and medical application.[3,4] The mycelium of *P. ostreatus* can be cultivated by submerged fermentation, which has the advantages of a short fermentation period, stable product spectrum, and easy industrial scale-up; it is therefore suitable for the research of medicinal substances and the relevant biosynthetic gene clusters. However, currently only about 14 terpenoids have been identified in *P. ostreatus*, 11 of them from liquid hyphae fermentation and three of them from the fruiting body (see Figure S1 in the Supporting Information).[5−8] These numbers are relatively low compared with other basidiomycete fungi. For example, at least 36 terpenoids have been isolated from the edible and medicinal basidiomycete fungi *Hericium erinaceus*.[9−11] Thus, activating silent genes and exploring the terpenoid diversity of *P. ostreatus* grown under liquid culture conditions is an important basis by which to understand its biosynthetic pathways and to develop new terpenoids as lead drugs.[12−14]

Several different strategies have been developed to activate the expression of silent genes in fungi cultured under laboratory conditions. These include genetic engineering, OSMAC (one strain many compounds), and coculture.[15,16] With recent rapid development of genetic tools in filamentous fungi, high expression of transcription factors and knockout of histone deacetylase genes have been widely used to broaden the structural diversity of secondary metabolites.[17,18] However, the genetic manipulation of basidiomycetes is substantially more complicated. Although the overexpression system or genetic editing by CRISPR-Cas9 has been established for a few basidiomycetes such as *P. ostreatus*, *Ganoderma* spp., and *Coprinopsis cinerea*,[19−21] it is still challenging to achieve the complete genetic functions of basidiomycetes due to the low efficiency of gene delivery and homologous recombination, and the lack of efficient genome editing elements. OSMAC is a simple and widely used strategy to enhance the structural diversity of secondary metabolites by altering culture conditions; however, its use is limited by its high degree of randomness.[22] The coculture strategy, which simulates the coexistence of microorganisms in nature, has been reported to activate a series of specific secondary metabolites through interspecific communication.[23] Our early research indicated

Received: May 17, 2023
Revised: June 28, 2023
Accepted: June 30, 2023
Published: July 13, 2023

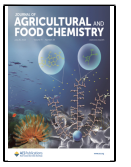

that utilizing different basidiomycetes as coculture pairs resulted in the stimulation of *P. ostreatus* to produce different antimicrobial substances.[4,6] As a result, we identified three unusual sesterterpenes (postredienes A−C, **PA−PC**) from *P. ostreatus* only when specifically cocultured with *Trametes robiniophila*.[6] However, these sesterterpenes were observed at low levels and some newly biosynthesized trace analogues could not be isolated under the specific culture conditions. As such, inspired by the OSMAC strategy, we hypothesized that by utilizing the generated postredienes as targets, an optimization of coculture conditions may not only increase the titers of **PA−PC** but also facilitate the discovery of additional novel terpenoids.

In the present study, genome mining analysis was first carried out to identify whether *P. ostreatus* possesses gene clusters that are rich enough to synthesize various terpenoids. We then optimized the coculture conditions to successfully increase the titers of **PA−PC** by over 2.5-fold and this facilitated the discovery of five new antimicrobial terpenoids, postredienes D−H (**1**−**5**). Their potential gene clusters and relevant biosynthetic pathways were further proposed based on analysis of structural features, gene functions, and RT-qPCR data. Overall, this study provides new avenues for the future study of terpenoid synthetic genes.

MATERIALS AND METHODS

General Experimental Procedures. NMR spectra were measured on a Bruker AVIII 500 MHz spectrometer (Bruker BioSpin International AG, Zurich, Switzerland). HRESIMS and ESIMS were acquired on a Thermo Orbitrap Fusion Lumos mass spectrometer (Thermo Fisher Scientific, Waltham, MA, USA) and an Agilent 1290/6460 mass spectrometer (Agilent Technologies Inc., Santa Clara, CA, USA), respectively. Specific rotations were acquired on a Hanon P850 automatic polarimeter (Haineng Future Technology Group Co., Ltd., Jinan, China). UV spectra were measured on a METASH UV-6000T spectrophotometer (Shanghai Metash Instruments Co., Ltd., Shanghai, China). Semipreparative HPLC was performed using an ODS column (YMC Co., Ltd., Kyoto, Japan). Column chromatography was performed using silica gel (ZCX-II, 200−300 mesh, Qingdao Marine Chemical Inc., Qingdao, China) and DAISOGEL SP-120-50-ODS-RPS (OSAKA SODA Co., Ltd., Osaka, Japan).[4] ECD spectra were acquired on a Chirascan CD spectrometer (Applied Photophysics Ltd., Surrey, UK).[4] Optimization experiments were designed and analyzed by Design-Expert V8.0.6.1 software (Stat-Ease, Inc., Minneapolis, MN, USA).

Basidiomycete Fungi. The strains SY10 and SY636 were collected from Qingdao, Shandong, China, and were identified as *P. ostreatus* (GenBank accession number OK442638) and *T. robiniophila* (GenBank accession number OR150202) by the ITS sequence, respectively. The strain *P. ostreatus* SY10 is deposited at the China Center for Type Culture Collection (CCTCC AF 2023044) and the strain *T. robiniophila* SY636 is deposited at the China General Microbiological Culture Collection Center (CGMCC 15274).

Genome Mining Analysis for Terpenoid Biosynthesis. Gene functions of *P. ostreatus* were predicted by antiSMASH (version 4.2.0) using the genome of *P. ostreatus* PC15 (GenBank assembly accession: GCA_000697685.1),[24] and gene clusters involved in terpenoid biosynthesis were analyzed by 2ndFind (http://biosyn.nih.go.jp/2ndFind/) and NCBI-BlastP (https://blast.ncbi.nlm.nih.gov/Blast.cgi?PAGE=Proteins).

Optimization of Coculture Conditions for Terpenoid Production. The coculture conditions were optimized using a single-factor test and Box−Behnken design (BBD). The single-factor test was utilized to study the culture medium and parameters.[25] The effects of carbon, nitrogen, and phosphorus sources as well as incubation temperature, initial pH, flask shaking speed, and volume of the culture medium on the production of **PA−PC** were inspected. The medium that was originally applied for the coculture of *P. ostreatus* SY10 and *T. robiniophila* SY636 leading to the discovery of **PA−PC** was used as the initial liquid medium (glucose 10.0 g/L, peptone 2.0 g/L, $MgSO_4{\cdot}7H_2O$ 0.5 g/L, KH_2PO_4 1.0 g/L, with a natural initial pH 5.0).[6] The coculture assays were performed according to the previously established method with slight modifications for cost saving.[6] Briefly, *P. ostreatus* SY10 and *T. robiniophila* SY636 were first cultured on a PDA solid medium for 7 days before three pieces of their mycelia of 6 mm in diameter were picked from the PDA plates and inoculated into flasks with 100 mL of liquid medium, respectively. After 7 days of monoculture, 100 mL of *T. robiniophila* SY636 fermentation broth was transferred into a 100 mL culture of *P. ostreatus* SY10 for further coculture. Similarly, when optimizing the volume of the culture medium, the two fungi were initially cultured separately with different volumes of the medium (i.e., 50, 75, 100, and 125 mL), and after 7 days' monoculture, the fermentation broth of *T. robiniophila* SY636 was transferred into the culture of *P. ostreatus* SY10 for further coculturing, and the medium volume then utilized was either 100, 150, 200, or 250 mL. All experiments were repeated at least twice. The fermentation broth was extracted by ethyl acetate (EtOAc), and analyzed by UPLC-MS to quantify **PB**, which was selected as the target compound for optimization. The data were presented as mean ± SD (shown as error bars in the figures). Within each set of experiments, Duncan's multiple range test was carried out using the statistical software SPSS (version 18.0). The letters mean difference among the groups, which were considered significant at $p < 0.05$.

Based on the results of the single-factor test, a BBD with three factors (A, B, and C) at three equidistant levels (−1, 0, and +1) was used to optimize the level of the key factors required for the maximal production of **PB** and its analogues.[26,27] The studied variables were the concentrations of glucose (A, at 30, 40, and 50 g/L), sucrose (B, at 10, 15, and 20 g/L), and peptone (C, at 4, 6, and 8 g/L). The experiment consisted of 17 combinations and the results obtained were analyzed by response surface methodology.

Fermentation, Extraction, and Isolation. Two fungi were further cocultivated at the optimized conditions. The whole broth (60 L) was filtered by a cheesecloth to separate the supernatant from the mycelia. The mycelia and supernatant were extracted with MeOH and EtOAc to give the organic extract (20.0 g).[4] The organic extract was first separated by a silica gel column using stepped gradient elution with the following solvents: petroleum ether (1 L), CH_2Cl_2 (1 L), 98:2 CH_2Cl_2−MeOH (2.5 L), 96:4 CH_2Cl_2−MeOH (2.5 L), 94:6 CH_2Cl_2−MeOH (2.5 L), 9:1 CH_2Cl_2−MeOH (5 L), and 1:1 CH_2Cl_2−MeOH (1 L), successively. This process resulted in the generation of seven fractions (fractions 1−7). Fraction 5 eluted with 94:6 CH_2Cl_2−MeOH was further subjected to a C-18 ODS column using a stepped gradient elution with MeOH−H_2O at different concentrations (5% 2 L, 20% 2.5 L, 40% 2.5 L, 60% 2.5 L, 80% 2.5 L, and 100% 2.5 L, successively). As a result, six subfractions (fractions 5-1−5-5) were obtained. Fraction 5-3 eluted with 40% MeOH−H_2O was fractionated by semipreparative HPLC with MeOH−H_2O (5 to 100%, 3 mL/min) to furnish four subfractions (fractions 5-3-1−5-3-4). Fraction 5-3-3 was further purified by semipreparative HPLC with MeOH-H_2O (22%, 3 mL/min) to obtain compounds **3** (8 mg, t_R = 45.4 min), **4** (6 mg, t_R = 46.7 min), and **5** (3 mg, t_R = 31.9 min). Fraction 5-5 eluted with 80% MeOH−H_2O was purified by semipreparative HPLC with MeOH−H_2O (70 to 100%, 3 mL/min) to obtain compounds **1** (15 mg, t_R = 22.4 min) and **2** (3 mg, t_R = 17.3 min).

*Postrediene D (**1**).* Colorless oil; $[\alpha]_D^{20}$ + 87.5 (*c* 0.1, MeOH); UV (MeOH) λ_{max} (log ε): 210 (3.20) nm; ^1H and ^{13}C NMR data, see Table 1; HRESIMS *m*/*z* 433.3287 $[M + Na]^+$ (calcd for $C_{25}H_{46}O_4Na^+$, 433.3288).

*Postrediene E (**2**).* Colorless oil; $[\alpha]_D^{20}$ + 49.5 (*c* 0.1, CH_3COCH_3); UV (MeOH) λ_{max} (log ε): 210 (3.20) nm; ^1H and ^{13}C NMR data, see Table 1; HRESIMS *m*/*z* 433.3288 $[M + Na]^+$ (calcd for $C_{25}H_{46}O_4Na^+$, 433.3288).

*Postrediene F (**3**).* Colorless oil; $[\alpha]_D^{20}$ − 454.0 (*c* 0.1, CH_3COCH_3); UV (MeOH) λ_{max} (log ε): 215 (3.79) nm; ^1H and

https://doi.org/10.1021/acs.jafc.3c03276
J. Agric. Food Chem. 2023, 71, 11110−11123

Table 1. ^{1}H (500 MHz) and ^{13}C (125 MHz) NMR Data for Compounds 1 and 2 (CD_3OD, δ ppm)

	1		2	
no.	δ_C	δ_H (J in Hz)	δ_C	δ_H (J in Hz)
1	25.9	1.67 s	25.9	1.67 s
2	132.1		132.0	
3	125.4	5.10 m	125.8	5.09 m
4	27.8	2.05−2.11 overlap	24.1	1.91−2.06 overlap
				1.81 m
5	40.9	1.97−2.05 overlap	45.6	1.46−1.56 overlap
				1.35−1.42 overlap
6	136.3		75.7	
7	125.6	5.17 m	55.1	1.91−2.06 overlap
8	26.2	2.20−2.28 overlap	23.9	1.91−2.06 overlap
		2.05−2.11 overlap		
9	32.2	1.56−1.61 overlap	31.0	1.91−2.06 overlap
		1.36−1.40 overlap		1.46−1.56 overlap
10	78.1	3.31 m	81.2	3.90 d (5.0)
11	75.4		49.6	
12	39.4	1.46 m	36.0	1.68−1.74 overlap
		1.56 m		1.35−1.42 overlap
13	22.9	2.05−2.11 overlap	23.7	1.91−2.06 overlap
14	126.2	5.21 m	126.8	5.19 m
15	135.9		135.4	
16	37.9	2.20−2.28 overlap	37.9	2.23 m
		1.97−2.05 overlap		1.91−2.06 overlap
17	30.8	1.31−1.36 overlap	30.7	1.68−1.74 overlap
		1.72 m		1.30−1.35 overlap
18	79.0	3.24 dd (10.6,1.6)	79.0	3.23 dd (10.5, 1.3)
19	73.1		74.8	
20	24.9	1.13 s	25.7	1.16 s
21	17.7	1.59 s	17.7	1.62 s
22	16.1	1.64 s	26.1	1.28 s
23	22.1	1.11 s	22.9	1.18 s
24	16.1	1.64 s	16.1	1.62 s
25	25.7	1.16 s	24.9	1.12 s

Table 2. ^{1}H (500 MHz) and ^{13}C (125 MHz) NMR Data for Compounds 3 and 4 (CD_3OD, δ ppm)

	3		4	
	δ_C	δ_H (J in Hz)	δ_C	δ_H (J in Hz)
1	131.3		131.3	
2	140.7	7.02 s	140.7	7.02 s
3	32.7	2.33−2.47 overlap	32.9	2.34−2.48 overlap
		2.07−2.15 overlap		2.04−2.16 overlap
4	40.1	2.15−2.27 overlap	40.2	2.16−2.27 overlap
5	28.8	1.92 m	28.7	1.92 m
		1.48 m		1.52 m
6	25.8	2.33−2.47 overlap	25.8	2.34−2.48 overlap
		2.15−2.27 overlap		2.16−2.27 overlap
7	170.8		170.8	
8	154.6		154.7	
9	33.0	2.33−2.47 overlap	33.1	2.34−2.48 overlap
		2.07−2.15 overlap		2.04−2.16 overlap
10	108.4	4.82 s	108.4	4.84 s
		4.81 s		4.82 s
11	31.0	1.78 m	31.0	1.80 m
		1.44 m		1.42 m
12	79.2	3.28 m	79.2	3.31 m
13	73.8		73.8	
14	25.7	1.18 d (4.8)	25.7	1.18 d (2.6)
15	24.8	1.14 d (4.9)	24.8	1.14 d (2.6)

Table 3. ^{1}H (500 MHz) and ^{13}C (125 MHz) NMR Data for Compound 5 (CD_3OD, δ ppm)

no.	δ_C	δ_H (J in Hz)
1	43.4	1.40 m
2	22.8	1.96 m
		1.34 m
3	25.9	2.39 m
		2.14 m
4	131.5	
5	142.5	7.18 s
6	39.2	2.30 m
7	47.3	1.12 m
8	20.5	1.62−1.68 overlap
		1.52−1.58 overlap
9	35.6	1.62−1.68 overlap
		1.52−1.58 overlap
10	73.5	
11	27.7	2.23 m
12	15.6	0.86 d (6.8)
13	21.7	0.98 d (6.7)
14	68.5	3.60 d (11.0)
		3.33 d (11.0)
15	171.2	

^{13}C NMR data, see Table 2; HRESIMS m/z 267.1608 $[M - H]^-$ (calcd for $C_{15}H_{23}O_4^-$, 267.1602).

Postrediene G (4). Colorless oil; $[\alpha]_D^{20}$ − 294.0 (c 0.1, MeOH); UV (MeOH) λ_{max} (log ε): 215 (3.80) nm; ^{1}H and ^{13}C NMR data, see Table 2; HRESIMS m/z 267.1607 $[M - H]^-$ (calcd for $C_{15}H_{23}O_4^-$, 267.1602).

Postrediene H (5). Colorless oil; $[\alpha]_D^{20}$ − 92.5 (c 0.1, $CHCl_3$); UV (MeOH) λ_{max} (log ε): 215 (3.85) nm; ^{1}H and ^{13}C NMR data, see Table 3; HRESIMS m/z 267.1608 $[M - H]^-$ (calcd for $C_{15}H_{23}O_4^-$, 267.1602).

Preparation of Methoxyphenylacetic Acid Esters Derived from PA. To the solutions of compound **PA** (3 mg each) in $CDCl_3$ (0.5 mL), (*R*)- or (*S*)-methoxyphenylacetic acid (MPA) (15 mg), DCC (15 mg), and DMAP (15 mg) were added.[28] The mixtures were stirred at room temperature for 1 h, then concentrated in vacuo, and purified by semipreparative HPLC (MeOH:H_2O = 50−100%) to yield the tri-(*R*)-MPA ester (**A1**) and tri-(*S*)-MPA ester (**A2**), respectively.

Tri-(*R*)-MPA ester (**A1**) is obtained as pale yellow oil; ESIMS m/z 887.5 $[M - H]^-$; ^{1}H and ^{13}C NMR data, see Table S1.

Tri-(*S*)-MPA ester (**A2**) is obtained as pale yellow oil; ESIMS m/z 887.5 $[M - H]^-$; ^{1}H and ^{13}C NMR data, see Table S1.

Preparation of the Acetonide Derivative Derived from 1. To the solution of compound **1** (5 mg) in $CDCl_3$ (0.2 mL), pyridinium *p*-toluene sulfonate (12 mg) and 2,2-dimethyoxypropane (800 μL) were added. The mixture was stirred at 35 °C for 16 h, then concentrated in vacuo, and purified by semipreparative HPLC (MeOH:H_2O = 50−100%) to yield the acetonide derivative **1a**, respectively.

Compound **1a** is obtained as pale yellow oil; ESIMS m/z 513.3 $[M + Na]^+$; ^{1}H and ^{13}C NMR data, see Table S2.

NMR Calculations. Spartan'14 software with the MMFF (Merck molecular force field) was used for conformational search. The conformers with high Boltzmann distribution (>5.0%) were reoptimized at the B3LYP/6-31+G (d) level using the Gaussian 09 program. Next, the NMR calculations of these conformers were performed using the gauge independent atomic orbital (GIAO) method at the mPW1PW91/6-311+G(d,p) level in MeOH with the polarizable continuum model (PCM).[4] The scaled chemical shifts

https://doi.org/10.1021/acs.jafc.3c03276
J. Agric. Food Chem. 2023, 71, 11110−11123

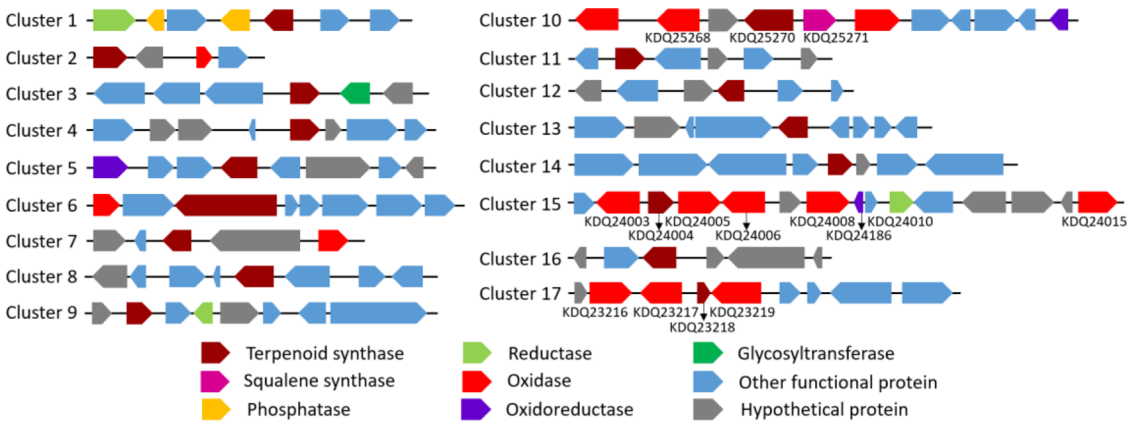

Figure 1. Seventeen putative gene clusters predicted for terpenoids biosynthesis.

(δ_s) of these conformers were calculated according to the equation proposed by Sarotti and co-workers.[29] The data of all the conformers were averaged based on their Boltzmann distribution at 298.15 K to obtain the final chemical shifts. The DP4+ probabilities of **2′a**−**2′h** were calculated based on shielding tensor using the Excel sheet provided by Sarotti and co-workers.[29,30]

Esterification of Compounds 3 and 4. To the solutions of compounds **3** or **4** (3.0 mg) in MeOH (0.5 mL), excess TMS-CHN_2 in *n*-hexane (200 μL) was added. The mixtures were stirred at room temperature for 2 h, then concentrated in vacuo, and purified by semipreparative HPLC (MeOH:H_2O = 50−100%) to yield methyl esters **3′** (2.0 mg) and **4′** (2.0 mg).[4]

Compound **3′** is obtained as pale yellow oil; ESIMS *m*/*z* 283.2 [M + H]$^+$; ^{1}H NMR (500 MHz, CD_3OD) δ 7.01 (m, 1H), 4.83 (s, 1H), 4.81 (s, 1H), 3.71 (s, 3H), 3.27 (dd, *J* = 10.6, 1.6 Hz, 1H), 2.34−2.47 (overlap, 3H), 2.16−2.24 (overlap, 2H), 2.05−2.16 (overlap, 2H), 1.92 (m, 1H), 1.78 (m, 1H), 1.49 (m, 1H), 1.42 (m, H), 1.17 (s, 3H), 1.14 (s, 3H).

Compound **4′** is obtained as pale yellow oil; ESIMS *m*/*z* 283.2 [M + H]$^+$; ^{1}H NMR (500 MHz, CD_3OD) δ 7.01 (m, 1H), 4.83 (s, 1H), 4.81 (s, 1H), 3.71 (s, 3H), 3.27 (dd, *J* = 10.2, 1.4 Hz, 1H), 2.35−2.48 (overlap, 3H), 2.17−2.27 (overlap, 2H), 2.05−2.14 (overlap, 2H), 1.91 (m, 1H), 1.78 (m, 1H), 1.50 (m, 1H), 1.41 (m, H), 1.17 (s, 3H), 1.14 (s, 3H).

Preparation of MPA Esters Derived from 3′ and 4′. To the solutions of compound **3′** (1.0 mg each) in $CDCl_3$ (0.5 mL), (*R*)- or (*S*)-MPA (5 mg), DCC (5 mg), and DMAP (5 mg) were added. The mixtures were stirred at room temperature for 1 h, then concentrated in vacuo, and purified by semipreparative HPLC (MeOH:H_2O = 50−100%) to yield the (*R*)-MPA ester (**3′a**) and (*S*)-MPA ester (**3′b**), respectively. Similarly, we obtained the (*R*)-MPA ester (**4′a**) and (*S*)-MPA ester (**4′b**) from **4′**.

*(R)-MPA Ester (**3′a**).* Pale yellow oil; ESIMS *m*/*z* 431.2 [M + H]$^+$; ^{1}H NMR (500 MHz, CD_3OD) δ 7.44−7.48 (overlap, 2H), 7.33−7.39 (overlap, 3H), 6.98 (m, 1H), 4.89 (s, 1H), 4.79 (s, H), 4.77 (s, H), 3.72 (s, 3H), 3.41 (s, 3H), 2.41 (m, 1H), 2.29 (m, 1H), 2.19 (m, 1H), 2.01−2.13 (overlap, 2H), 1.89−1.99 (overlap, 3H), 1.83 (m, 1H), 1.63 (m, 1H), 1.38 (m, 1H), 0.95 (s, 3H), 0.84 (s, 3H).

*(S)-MPA Ester (**3′b**).* Pale yellow oil; ESIMS *m*/*z* 431.2 [M + H]$^+$; ^{1}H NMR (500 MHz, CD_3OD) δ 7.45−7.49 (overlap, 2H), 7.30−7.39 (overlap, 3H), 6.93 (m, 1H), 4.91 (s, 1H), 4.66 (s, H), 4.56 (s, H), 3.73 (s, 3H), 3.39 (s, 3H), 2.33 (m, 1H), 2.04−2.15 (overlap, 2H), 1.78−1.88 (overlap, 3H), 1.75 (m, 1H), 1.56−1.63 (m, 1H), 1.45−1.56 (overlap, 2H), 1.34−1.41 (m, 1H), 1.18 (s, 3H), 1.17 (s, 3H).

*(R)-MPA Ester (**4′a**).* Pale yellow oil; ESIMS *m*/*z* 431.2 [M + H]$^+$; ^{1}H NMR (500 MHz, CD_3OD) δ 7.45−7.49 (overlap, 2H), 7.30−7.38 (overlap, 3H), 6.92 (m, 1H), 4.91 (s, 1H), 4.66 (s, H), 4.55 (s, H), 3.73 (s, 3H), 3.39 (s, 3H), 2.35 (m, 1H), 2.12 (m, 1H), 2.04 (m, 1H), 1.71−1.84 (overlap, 4H), 1.63 (m, 1H), 1.54 (m, 1H), 1.46 (m, 1H), 1.35 (m, 1H), 1.18 (s, 3H), 1.17 (s, 3H).

*(S)-MPA Ester (**4′b**).* Pale yellow oil; ESIMS *m*/*z* 431.2 [M + H]$^+$; ^{1}H NMR (500 MHz, CD_3OD) δ 7.44−7.49 (overlap, 2H), 7.32−7.39 (overlap, 3H), 6.98 (m, 1H), 4.89 (s, 1H), 4.80 (s, H), 4.77 (s, H), 3.72 (s, 3H), 3.41 (s, 3H), 2.41 (m, 1H), 2.29 (m, 1H), 2.19 (m, 1H), 1.88−2.12 (overlap, 5H), 1.81 (m, 1H), 1.63 (m, 1H), 1.39 (m, 1H),0.95 (s, 3H), 0.84 (s, 3H).

ECD Calculations. Spartan′14 software with the MMFF was used for conformational search. The conformers with high Boltzmann distribution (>5.0%) were reoptimized at the B3LYP/6-31+G (d) level using the Gaussian 09 program. Next, the TDDFT calculations of these conformers were performed using 30 excited states at the B3LYP/6-31+G (d) level in MeOH with PCM. ECD spectra were generated using the program SpecDis by applying a Gaussian band shape with a 0.2 (for **3″**) and 0.4 eV (for **5**) width from dipole-length rotational strengths. The dipole velocity forms yielded negligible differences. The calculated spectra were blue-shifted by 30 (for **3″**) and 23 nm (for **5**) to facilitate comparison to the experimental data.

Assay of Antimicrobial Activity. The antimicrobial assays of isolated compounds **1**−**5** against six microorganisms, including two fungi, *Candida albicans* (ATCC 10231) and *Cryptococcus neoformans* (ATCC 90012); two Gram-positive bacteria, *Bacillus subtilis* LAM-1001 (CCTCC AB 2023141) and *Staphylococcus aureus* LAM-1002 (ATCC 29213); and two Gram-negative bacteria, *Escherichia coli* LAM-1003 (CCTCC AB 2023143) and *Shigella* sp. LAM-1004 (CCTCC AB 2023142), were performed using the broth microdilution method in 96-well plates, as previously reported with slight modification.[6,31] Briefly, solutions of compounds **1**−**5** (10.0 or 30.0 mg/mL) and positive control drugs ciprofloxacin (0.8 mg/mL) and amphotericin B (5.0 mg/mL) were made up in MeOH or DMSO and dispensed into 96-well plates using the 2× microdilution method. After incubation at 37 °C for 12−24 h, the optical densities of microorganisms were measured at 600 nm to calculate MIC_{80} values (the concentrations at which the isolated compounds inhibited the growth of microorganisms by 80%).

RT-qPCR Analysis. The mycelium pellets of *P. ostreatus* SY10 were harvested from the coculture and monoculture broth on day 14 for RNA extraction.[6] Total RNA were obtained from three biological replicates by using a RC401 FastPure Plant Total RNA Isolation kit (Vazyme, Nanjing, China). The quality and quantity of RNA were analyzed by a Microvolume UV−is spectrophotometer (Thermo Fisher, CA, USA). The cDNA was obtained via reverse transcription by using 1 μg of RNA and a R323-01 HiScript III RT SuperMix (Vazyme, Nanjing, China). Then, real-time RT-qPCR was performed using the obtained cDNA, the primer pairs (Table S3), and AceQ Universal SYBR qPCR Master Mix (Vazyme, Nanjing, China) with β-tubulin genes used as a reference gene.[6] Three biological replicates were performed for each reaction. The relative expression levels of the target genes were analyzed using the $2^{-\Delta\Delta CT}$ method.[32]

https://doi.org/10.1021/acs.jafc.3c03276
J. Agric. Food Chem. 2023, 71, 11110−11123

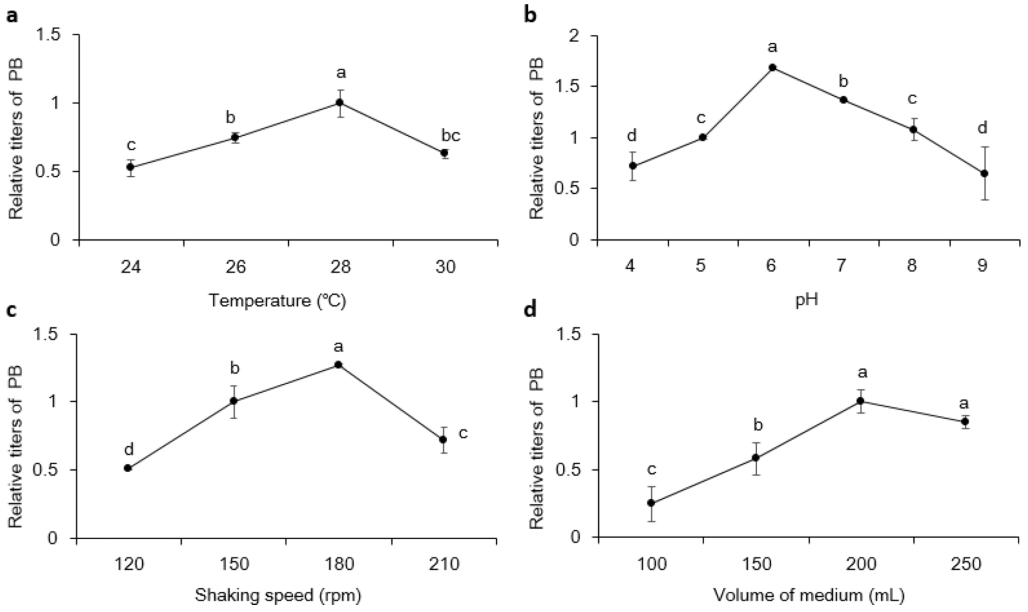

Figure 2. Effects of incubation temperature (a), initial pH (b), flask shaking speed (c), and volume of culture (d) on the titer of **PB**. The average titer of **PB** at initial conditions was set to 1.

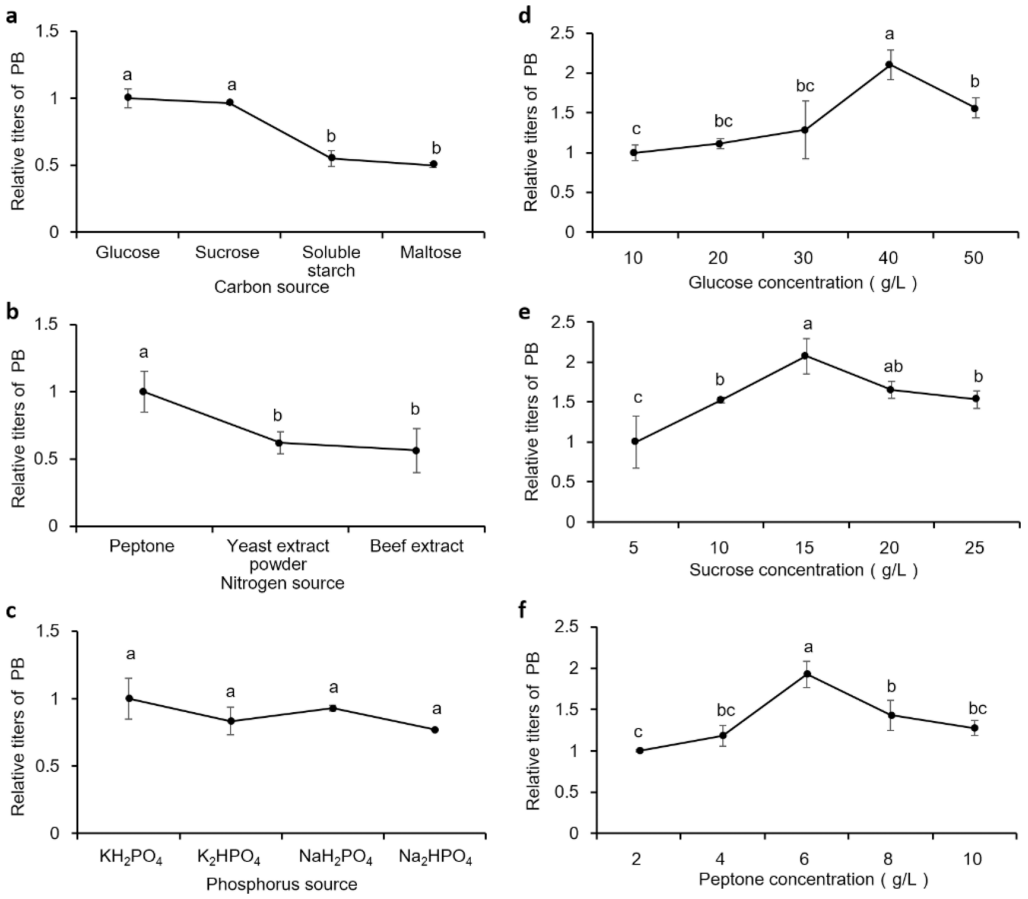

Figure 3. (a–c) Effects of different carbon, nitrogen, and phosphorus sources on the titer of **PB**. (d–f) Effects of different concentrations of glucose, sucrose, and peptone on the titer of **PB**. The average titer of **PB** at initial conditions was set to 1.

RESULTS AND DISCUSSION

Gene Cluster Mining for Terpenoid Biosynthesis. Gene cluster mining of *P. ostreatus* was performed by AntiSMASH using the genome of *P. ostreatus* PC15,[24] a strain that exhibits high identity with *P. ostreatus* SY10.[6] The results indicated that 17 putative gene clusters are involved in terpenoid biosynthesis, and at least 10 clusters possess multiple genes that may contribute to the structural modification of terpenoids (Figure 1). Our previous study indicated that

https://doi.org/10.1021/acs.jafc.3c03276
J. Agric. Food Chem. 2023, 71, 11110−11123

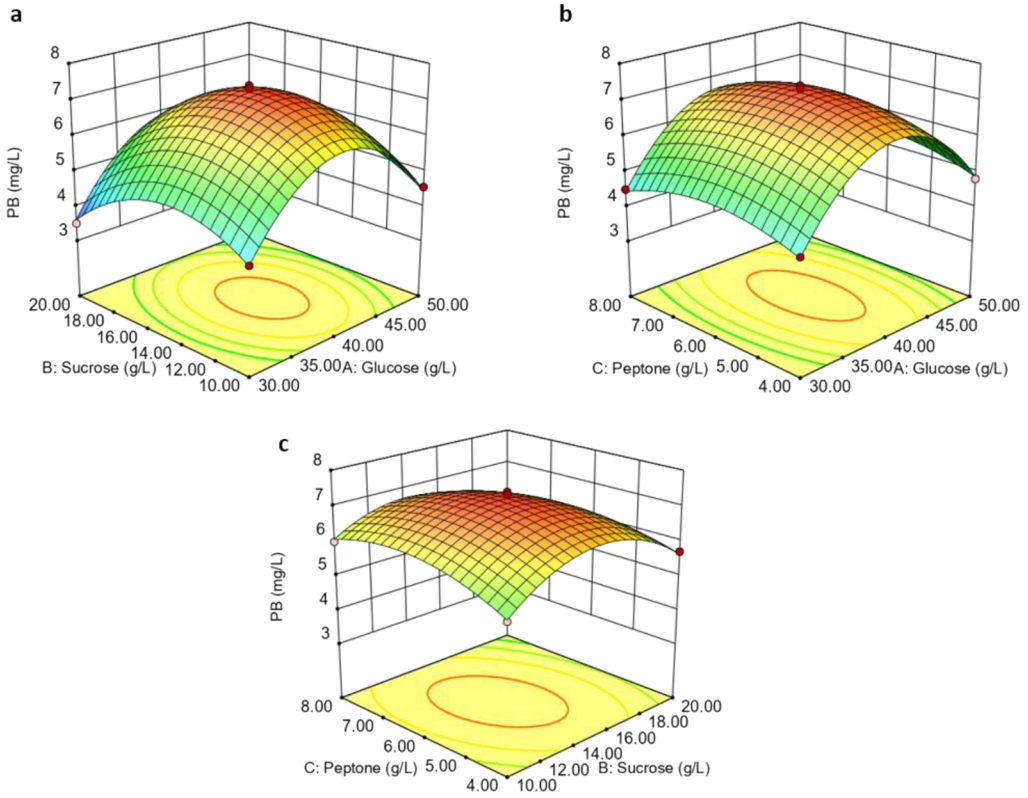

Figure 4. Response surface plots showing the effect of cross-interactions among the concentrations of glucose (A), sucrose (B), and peptone (C) on the titer of **PB**.

cluster 10 is capable of synthesizing the unusual sesterterpenes **PA**−**PC**. Moreover, cluster 10 is proposed to likely produce a series of additional compounds, as it possesses 11 putative functional genes encoding at least one short chain oxidoreductase, and three oxidases including two monooxygenases and one squalene epoxidase (Figure 1 and Table S4). In addition, clusters 15 and 17 with a length of 41.3 and 23.4 kb, respectively, are predicted to have 9 and 15 functional genes. Both clusters are predicted to have at least three genes responsible for structural modification, such as genes encoding cytochrome P450, alcohol oxidase, dehydrogenase, oxidoreductase, and aldo-keto reductase (Figure 1 and Table S4). Clusters 15 and 17 shared low similarity with currently known gene clusters (Table S4), suggesting a high likelihood of synthesizing new terpenoids in *P. ostreatus*. As such, bioinformatic analysis confirmed that *P. ostreatus* has an abundant genetic basis by which to generate various terpenoids.

Optimization of Coculture Conditions to Increase Terpenoid Synthesis. Guided by the OSMAC strategy, coculture conditions for *P. ostreatus* SY10 and *T. robiniophila* SY636 were optimized to enhance the titers of **PA**−**PC** and induce the structural diversity of terpenoids using a single-factor test and BBD. **PB**, which exhibited a higher production level of 3.28 mg/L at initial coculture conditions and significant bioactivities against human pathogenic fungi *C. albicans* and *C. neoformans*, was selected as the target compound for guiding the optimization. Since terpenoids are derived from the same precursor, namely, C_5 isoprene units, we speculated that this optimization strategy would most likely increase the synthesis of additional terpenoids.

First, we focused on optimizing the culture medium and parameters using a single-factor test. The tested parameters included carbon, nitrogen, and phosphorus sources, in addition to incubation temperature, initial pH, flask shaking speed, and culture volume. These conditions have been reported to have significant effects on secondary metabolite production in fungi.[25,26,33,34] *P. ostreatus* SY10 and *T. robiniophila* SY636 were first cultured separately for 7 days to obtain the necessary biomass. Next, a fermentation broth of *T. robiniophila* SY636 was transferred into the culture of *P. ostreatus* SY10 for further coculturing. After 7 days of fungi−fungi interactions, the levels of the desired target compound **PB** were measured by UPLC-MS. The production levels were displayed as relative titers of **PB**, with the average titer of **PB** under initial conditions set to 1. Our results revealed that the maximum titers of **PB** were obtained at 28 °C, an initial pH 6.0, 180 rpm, and 200 mL of the culture medium (Figure 2). Compared to the initial culture conditions, namely, 28 °C, pH 5.0, 150 rpm, and 200 mL, the optimized pH and shaking speed were higher. These findings suggested that appropriate increases in pH and dissolved oxygen (DO) were beneficial to the synthesis of this kind of terpenoid. These results were consistent with those observed for the biosynthesis of triterpene acids in *Ganoderma lingzhi*, whereby the optimal conditions were an initial pH of 5.9 and 20% DO in a bioreactor.[35] In addition, the single-factor test for carbon, nitrogen, and phosphorus sources suggested that two types of carbon sources, i.e., glucose and sucrose (no significant difference between the two), and one type of nitrogen source, i.e., peptone, resulted in production of the highest titers of **PB** (Figure 3a,b). Meanwhile, the type of phosphorus source had no obvious effect on the **PB** titer (Figure 3c); thus, we maintained the original component

https://doi.org/10.1021/acs.jafc.3c03276
J. Agric. Food Chem. 2023, 71, 11110−11123

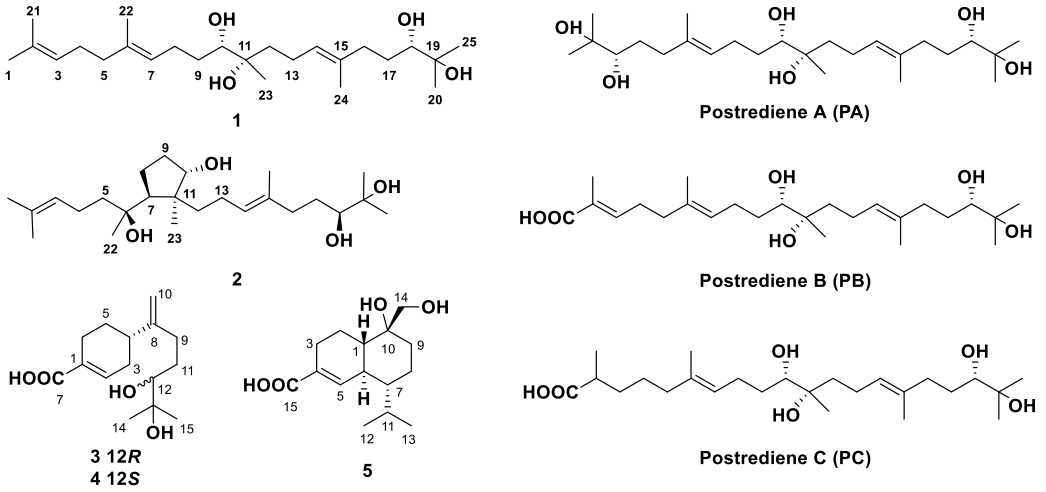

Figure 5. Structures of compounds **1**−**5** and postredienes A−C.

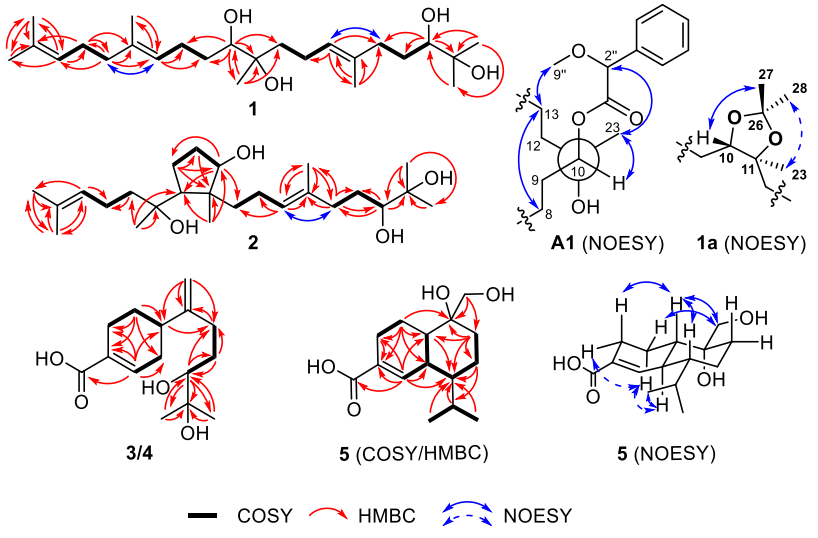

Figure 6. Key COSY, HMBC, and NOESY correlations of **1**−**5**, **A1**, and **1a**.

KH_2PO_4. Based on these results, the optimized levels were further examined to determine the center points for a BBD. The results indicated that the optimized concentrations of glucose, sucrose, and peptone were 40, 15, and 6 g/L (Figure 3d−f), respectively, while the concentration of KH_2PO_4 had no obvious influence on the **PB** titer (Figure S2). Glucose, sucrose, and peptone were also reported as the optimum carbon and nitrogen source for terpenoid generation in other basidiomycete fungi;[34,36,37] however, there were few reports about the effects of phosphorus sources on the biosynthesis of terpenoids in basidiomycetes.

Based on the results of the single-factor test, glucose, sucrose, and peptone were further utilized as the key variable factors for a BBD.[25,26] The concentration levels were set to: glucose (A, at 30, 40, and 50 g/L), sucrose (B, at 10, 15, and 20 g/L), and peptone (C, at 4, 6, and 8 g/L). The experiment consisted of 17 different combinations, and the corresponding titers of **PB** are described in Table S5. The variance analysis of the regression model is shown in Table S6. The "*P*-value" is <0.0001, and the "Lack of Fit *P*-value" is 0.6637, revealing that the regression equation is extremely significant and the experimental method is reliable. The parameters A, B, BC, A^2, B^2, and C^2 are all significant ($P < 0.05$), indicating that three key factors significantly influence the model. The "Adeq Precision" ratio of 31.179 is higher than the 4.0 cutoff, and this indicates high reliability of the model. According to the regression equation, analysis charts were generated (Figures 4 and S3). The profiles of the response surfaces are all convex with a downward open direction (Figure 4) and the contour lines are oval with the contour centers located in the set range (Figure S3), which indicates the interactions between the three factors and the existence of the highest point of the response value.[25,26] Utilizing the Box−Behnken experiment of response surface methodology, an optimized culture medium was finally developed: 45.50 g/L glucose, 14.50 g/L sucrose, and 6.00 g/L peptone, with other ingredients unchanged, namely, 0.50 g/L $MgSO_4{\cdot}7H_2O$ and 1.00 g/L KH_2PO_4, and these parameters were predicted to result in an optimal **PB** titer of 6.70 mg/L. A verification test under the optimized coculture conditions (28 °C, an initial pH 6.0, 180 rpm, and 200 mL of the optimized culture medium) indicated that the titer of **PB** could be increased to 8.40 mg/L after culturing for 14 days, which was 2.56 times higher than the titer of **PB** grown under initial coculture conditions. Meanwhile, the titers of **PA** and **PC** were increased to 3.14 and 1.28 mg/L, respectively, 2.74 and 2.53 times higher than the titers under initial coculture conditions.

https://doi.org/10.1021/acs.jafc.3c03276
J. Agric. Food Chem. 2023, 71, 11110−11123

The noticeable increase in titers was in agreement with the model and comparable to those reported in other literature studies. For example, it has been reported that the titers of triterpene acids in *Ganoderma* fungi were increased by up to 1.3−2.5-fold through the optimization of culture conditions or the medium using the single-factor test and the Box−Behnken experiment.[35−38] Our results suggest that optimization of coculture conditions is an effective strategy by which to increase terpenoid biosynthesis.

Structure Elucidations of New Terpenoids and Evaluation of Antimicrobial Activity. Guided by genome analysis data, we speculated that *P. ostreatus* possesses abundant terpenoid-associated gene clusters with great potential to generate diverse terpenoids. Thus, terpenoids with a typical absorption of 215 nm were excavated on the basis of optimized cocultivation. As a result, five new terpenoids were isolated, including two new sesterterpenes named postredienes D (**1**) and E (**2**), as well as three new sesquiterpenes named postredienes F−H (**3**−**5**) (Figure 5).

Compound **1** was isolated as colorless oil, with a molecular formula of $C_{25}H_{46}O_4$ deduced from the HREIMS peak at *m*/*z* 433.3287 $[M + Na]^+$. The 1D NMR spectroscopic data (Table 1) of **1** indicated the presence of three sp^2 nonprotonated carbons (δ_C 132.1, 136.3, and 135.9), two oxygenated sp^3 nonprotonated carbons (δ_C 75.4 and 73.1), three sp^2 methines (δ_C 125.4, 125.6, and 126.2), two oxygenated sp^3 methines (δ_C 78.1 and 79.0), eight sp^3 methylenes, and seven methyls, which are similar to those of the sesterterpenes **PA**−**PC** we have previously reported (Figure 5). Careful inspection of 1D NMR spectra revealed that clear obvious differences with **PA** included the presence of signals for an additional double bond and the absence of signals for two oxygenated carbons. Further analysis of the 2D NMR spectra indicated that the additional double bond (δ_C 132.1 and 125.4) is located at C-2 and C-3 in compound **1**, while the two hydroxyl groups at C-2 and C-3 in **PA** are absent in **1**. The NOESY correlations from H_2-5 to H-7 and from H-14 to H_2-16 suggested the *trans* configurations of the double bonds at C-6 and C-14 (Figure 6). The other configurations of **1** were speculated to be the same as those of **PA** based on the same biogenetic origin. **PA** possesses one more chiral center than compound **1**. However, the configurations of **PA** were not completely determined previously due in part to its limited production. Thus, we attempted to determine the configurations of this class of compounds by making the MPA esters and acetonide derivatives,[39,40] as well as conducting conformational analysis, using **PA** or **1**.

First, the absolute configurations of 3-OH, 10-OH, and 18-OH in **PA** were determined by making the MPA esters. Via the reactions between **PA** and (*R*/*S*)-MPA, we obtained **A1** (a tri-(*R*)-MPA ester of **PA** on C-3, C-10, and C-18) and **A2** (a tri-(*S*)-MPA ester of **PA** on C-3, C-10, and C-18), respectively. The proton signals around C-3, C-10, and C-18 of both derivatives were assigned by 1D and 2D NMR data (Table S1 and Figure S4).[40] The $\Delta\delta^{RS}$ values of **A1** and **A2** are negative for H_2-5, H-7, H_2-8, H-14, H_2-16, H_3-22, and H_3-24 and positive for H-1, H_2-12, H_3-20, H_3-21, H_3-23, and H_3-25 (Figure 7a), indicating the 3*S*, 10*S*, and 18*S* configurations. The absolute configuration of C-11 can be preliminarily inferred by conducting conformational analysis of **A1**.[41] As shown in Newman projection of **A1** (Figure 6), the NOESY correlations between H_2-13 and H_2-8/H-9″ and between H_3-23 and H-10/H-2″ revealed a *threo* configuration between the

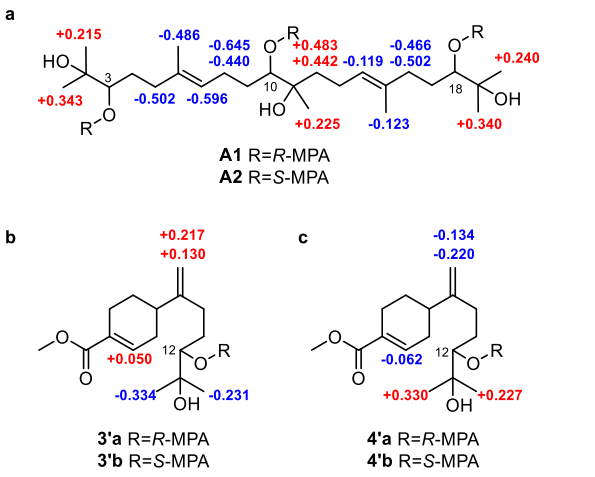

Figure 7. $\Delta\delta^{RS}$ values between **A1** and **A2** (a), between **3′a** and **3′b** (b), and between **4′a** and **4′b** (c).

hydroxyl groups at C-10 and C-11, which suggested the *S* configuration of C-11. We further made the acetonide derivative (**1a**) of compound **1** to prove this conclusion.[39] The proton signals around C-11 of **1a** were assigned by 1D and 2D NMR data (Table S2 and Figure S5). The NOESY spectrum showed correlations between H-10 (δ_H 3.75) and H_3-27 (δ_H 1.33) and between H_3-23 (δ_H 1.21) and H_3-28 (δ_H 1.39), which provided additional evidence supporting the *S* configuration of C-11 (Figure S5). Thus, the full absolute configurations of **PA** were determined to be 3*S*, 10*S*, 11*S*, and 18*S*, and the configurations of **1** were speculated to be the same as **PA**, that is, 10*S*, 11*S*, and 18*S*, according to the same biogenetic origin.

Compound **2** was isolated as pale yellow oil, with a molecular formula of $C_{25}H_{46}O_4$ that was deduced from the HREIMS peak at *m*/*z* 433.3288 $[M + Na]^+$. The 1D NMR spectroscopic data (Table 1) of **2** indicated the presence of two sp^2 nonprotonated carbons (δ_C 132.0 and 135.4), three sp^3 nonprotonated carbons including two oxygenated (δ_C 75.7 and 74.8), two sp^2 methines (δ_C 125.8 and 126.8), three sp^3 methines including two oxygenated (δ_C 81.2 and 79.0), eight sp^3 methylenes, and seven methyls, which are similar to those of compound **1**. Comparison of 1D NMR spectra revealed that compound **2** possesses two more signals for sp^3 carbons than compound **1**, while lacking two signals for sp^2 carbon. The HMBC correlations from H_3-22 to C-5/C-6/C-7, from H_3-23 to C-7/C-10/C-11, from H_2-8 to C-9/C-10/C-11, from H_2-9 to C-11, and from H-10 to C-7/C-8/C-12 indicated that a five-membered ring (C-7 to C-11) is present in compound **2** instead of the linear structure with double bonds at C-6 in compound **1**. The NOESY correlation from H-14 to H_2-16 suggested a *trans* configuration of the double bond at C-14 (Figure 6). The absolute configurations of the 10-OH and 18-OH of **2** were speculated to be the same as those of **PA** according to the same biogenetic origin, that is, 10*S* and 18*S*. The absolute configurations of other chiral centers, including C-6, C-7, and C-11, were determined by NMR calculations using the fragments **2′a**−**2′h** as the truncated model structures of **2** (Figure 8).[39] The experimental and calculated ^1H and ^{13}C NMR data were compared by DP4+ probability analysis (Figure 8 and Table S7) and **2′a** with a high probability of 87.59% was predicted to be correct, suggesting the 6*S*, 7*S*, and

https://doi.org/10.1021/acs.jafc.3c03276
J. Agric. Food Chem. 2023, 71, 11110−11123

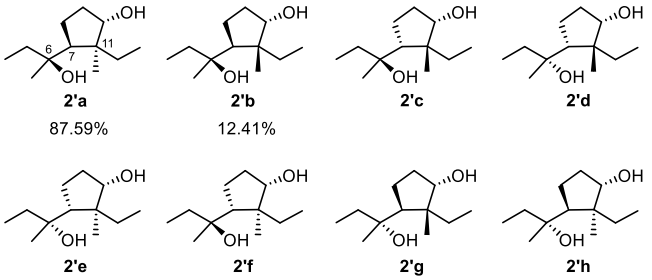

Figure 8. Calculated DP4+ probabilities of **2′a**−**2′h**, based on ^{1}H and ^{13}C NMR data.

11*S* configurations for compound **2**. Thus, the full absolute configurations of compound **2** were determined.

Compounds **3** and **4** were both isolated as colorless oil, with the same molecular formula of $C_{15}H_{24}O_4$ that was deduced from the HREIMS peaks at *m*/*z* 267.1608 $[M - H]^-$ or 267.1607 $[M - H]^-$. The 1D NMR spectroscopic data (Table 2) of compounds **3** and **4** both indicated the presence of four nonprotonated carbons including one carbonyl (δ_C 170.8), one sp^2 methine (δ_C 140.7), two sp^3 methines including one oxygenated (δ_C 79.2), one sp^2 methylene (δ_C 108.4), five sp^3 methylenes, and two methyls. Next, we comprehensively analyzed the 2D NMR data of compound **3** (Figure 6). The COSY correlations between H-2 and H_2-3, between H-4 and H_2-5, and between H_2-5 and H_2-6, along with the HMBC correlations from H-2 to C-1/C-3/C-4/C-6 and from H_2-5 to C-1/C-3/C-4/C-6, indicated the presence of a bisubstituted cyclohexene fragment. The COSY correlations between H_2-9 and H_2-11 and between H_2-11 and H-12, along with the HMBC correlations from H_2-10 to C-4/C-8/C-9, from H-4 to C-9, from H_2-11 to C-9/C-12, from H-12 to C-9/C-11/C-13/C-14/C-15, from H_3-14 to C-12/C-13, and from H_3-15 to C-12/C-13, indicated that a C_8 side chain (C-8−C-15) is attached on C-4 of the cyclohexene fragment. In addition, comprehensive analysis of the HMBC correlation from H-2 to C-7, as well as the molecular formula and the chemical shifts of C-7 (δ_C 170.8), C-12 (δ_C 79.2), and C-13 (δ_C 73.8), suggested that a carboxyl group is attached on C-1 of the cyclohexene fragment and furthermore that both C-12 and C-13 are connected with a hydroxyl group. Thus, the planar structure of **3** was determined as shown in Figure 5. It shares the same scaffold with hamanasic acid A and elgonene C but exhibits differences in substituents.[42,43] Further analysis of the 2D NMR data of compound **4** indicated that it shares the same planar structure as **3**.

The configurations of **3** and **4** were determined by making the MPA esters, CD experiment, and density functional theory calculation of ECD data. First, the absolute stereochemistry at C-12 was determined by making the MPA esters.[28,39] To avoid the influence of the carboxylic acid group, compounds **3** and **4** were esterified to generate methyl ester (**3′** and **4′**). Next, **3′** and **4′** were used to react with (*R*/*S*)-MPA to obtain **3′a**/**4′a** ((*R*)-MPA esters of **3′**/**4′** on C-12) and **3′b**/**4′b** ((*S*)-MPA esters of **3′**/**4′** on C-12), respectively. The $\Delta\delta^{RS}$ values between **3′a** and **3′b** are negative for H_3-14 and H_3-15 and positive for H_2-10 and H-2 (Figure 7b), indicating the 12*R* configuration, while the $\Delta\delta^{RS}$ values between **4′a** and **4′b** are positive for H_3-14 and H_3-15 and negative for H_2-10 and H-2 (Figure 7c), indicating the 12*S* configuration. In addition, to determine the absolute stereochemistry at C-4, the ECD spectrum of compound **3** was obtained using the truncated fragment **3″** as the model structure (Figure S6).[44] As shown in Figure 9a, the calculated ECD spectrum of 4*S*-**3″** shows similar Cotton effects with the experimental spectra of **3** and **4**. Based on the above evidence, the full absolute configurations of **3** and **4** were determined to be 4*S*, 12*R* and 4*S*, 12*S* respectively.

Compound **5** was isolated as colorless oil, with a molecular formula of $C_{15}H_{24}O_4$ that was deduced from the HREIMS peak at *m*/*z* 267.1608 $[M - H]^-$. The 1D NMR spectroscopic data (Table 3) of **5** indicated the presence of three nonprotonated carbons including one carbonyl (δ_C 171.2), one sp^2 methine (δ_C 142.5), four sp^3 methines, five methylenes including one oxygenated methylene (δ_C 68.5), and two methyls. The COSY correlations between H_2-2 and H_2-3, between H-6 and H-1/H-5/H-7, and between H_2-8 and H-7/H_2-9, along with the HMBC correlations from H-2 to C-1/C-3/C-4/C-6, from H-5 to C-1/C-3/C-4/C-6/C-7, from H_2-9 to C-1/C-7/C-8/C-10, and from H-1 to C-7, indicated the existence of a tetra-substituted octahydronaphthalene scaffold (Figure 6). The COSY correlations between H-11 and H_3-12/H_3−13 and the HMBC correlations from H_3-12/H_3-13/H-11 to C-7 indicated that an isopropyl group (C-11−C-13) is attached on C-7 of the tetra-substituted octahydronaphthalene scaffold. In addition, according to the HMBC correlations from H_2-14 to C-9/C-10 and from H-5 to C-15, as well as the molecular formula and the chemical shifts of C-10 (δ_C 73.5), C-14 (δ_C 68.5), and C-15 (δ_C 171.2), we deduced that one

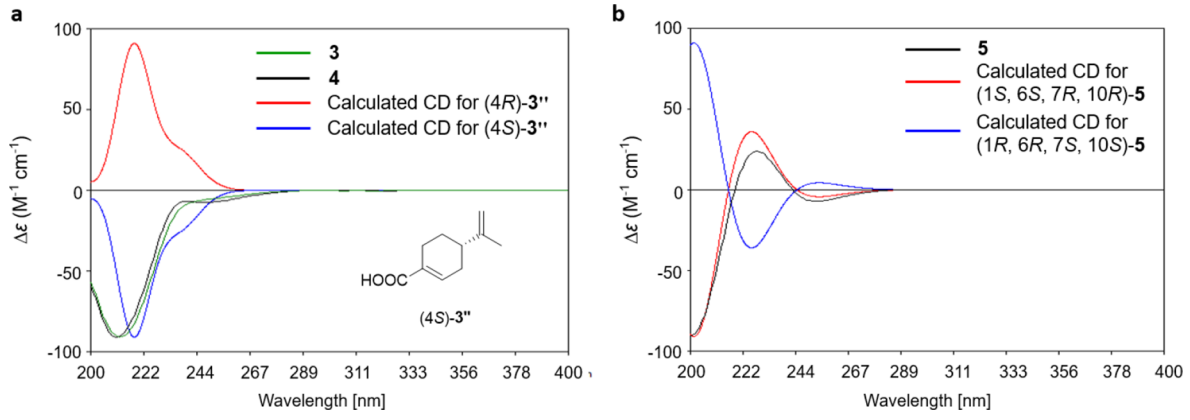

Figure 9. (a) Experimental ECD spectra of compounds **3** and **4** and the calculated spectra for (4*S*)- and (4*R*)-**3″**. (b) Experimental ECD spectrum of compound **5** and the calculated spectra for (1*S*,6*S*,7*R*,10*R*)-**5** and (1*SR*,6*R*,7*S*,10*S*)-**5**.

https://doi.org/10.1021/acs.jafc.3c03276
J. Agric. Food Chem. 2023, 71, 11110−11123

carboxyl group is attached on C-1, while one hydroxyl group and one hydroxymethyl group are attached on C-10. Thus, the planar structure of **5** was determined as shown in Figure 5. It shares the same scaffold with rhinomilisin G and 12-hydroxy-α-cadinol but exhibits differences in substituents.[45,46] The relative configurations of compound **5** were determined by NOESY correlations between H-2α and H-3α/H-6, between H-1 and H-7/H-3β, between H_2-14 and H-2β/H-1, and between H-6 and H_3-12 (Figure 6). The absolute configurations of **5** were determined by comparing its experimental and calculated ECD spectra. The calculated ECD spectrum of (1*S*,6*S*,7*R*,10*R*)-**5** shows the positive Cotton effect near 225 nm and the negative Cotton effect around 250 nm, which closely matches the experimental one (Figures 9b and S7). Thus, the full absolute configurations of **5** were determined to be 1*S*, 6*S*, 7*R*, 10*R*.

The antimicrobial activities of the five new compounds were tested against six microorganisms including two fungi, *C. albicans* and *C. neoformans*; two Gram-positive bacteria, *B. subtilis* and *S. aureus*; and two Gram-negative bacteria, *E. coli* and *Shigella* sp. Ciprofloxacin and amphotericin B were used as positive control drugs. All analyzed compounds showed obvious antimicrobial activities against fungi or Gram-positive bacteria. Among them, compound **1** exhibited significant activities against the human pathogenic fungi *C. albicans* and *C. neoformans* with MIC_{80} values of 0.9 and 1.1 μg/mL, which are comparable to those of amphotericin B (Table 4). These results revealed the potential of these compounds to inhibit human pathogenic fungi and G^+ bacteria.

Table 4. Antimicrobial Activities (MIC_{80}) of Compounds 1−5[a]

	MIC_{80} (μg/mL)			
comp.	*C. albicans*	*C. neoformans*	*B. subtilis*	*S. aureus*
1	0.9	1.1	38.9	>150
2	3.1	40.0	91.8	>150
3	>150	>150	41.6	150
4	>150	>150	49.5	>150
5	>150	33.2	43.6	>150
amphotericin B	0.4	0.8		
ciprofloxacin			0.6	2.3

[a]Note: amphotericin B and ciprofloxacin were used as positive control drugs for antifungal and antibacterial activity, respectively.

Possible Gene Clusters for Synthesizing Compounds 1−5 and the Relevant Biosynthetic Pathway. The UPLC-MS analysis revealed that compounds **1**−**5** were undetectable in the monoculture broth of *T. robiniophila* SY636, while could be detected in the monoculture broth of *P. ostreatus* SY10 with the titers significantly increased in the coculture (Figure S8). These findings indicate that the expression levels of their biosynthetic genes in *P. ostreatus* SY10 were upregulated by coculturing with *T. robiniophila* SY636 under optimal coculture conditions. Structural analysis of compounds **1**−**5** indicated that they are all terpenoids synthesized from C_5 isoprene units. In the biosynthesis of the known terpenoids, prenyltransferases generally link the C_5 precursors in a head-to-tail manner to form linear isoprenoid precursors of various lengths, such as geranyl diphosphate (GPP; C_{10}), farnesyl diphosphate (FPP; C_{15}), geranylgeranyl diphosphate (GGPP; C_{20}), and geranylfarnesyl diphosphate (GFPP; C_{25}).[47−49] However, compounds **1** and **2**, as well as **PA**−**PC**, share an unusual C_{25} precursor, which are probably synthesized from GPP and FPP fragments in a tail-to-tail manner, similarly to the synthesis of squalene from two molecules of FPP. We speculated that compounds **1** and **2** were biosynthesized by cluster 10 (Table S4), which was proposed to be responsible for the synthesis of **PA**−**PC** based on transcriptome and RT-qPCR analyses in our previous study.[6] Compounds **3**−**5** are sesquiterpenes originating from the same C_{15} precursor FPP, with a carboxyl group and two adjacent hydroxyl groups in structures. The structural features suggested that there should be at least two oxidases in the biosynthetic gene cluster associated with compounds **3**−**5** to catalyze the formation of carboxyl and hydroxyl groups, respectively; thus, clusters 15 and 17 (Table S4), which possess a putative terpenoid synthase, cytochrome P450, and many other oxidases, were considered as candidate gene clusters.

To further investigate the biosynthetic gene clusters for compounds **1**−**5**, the transcriptional levels of the gene clusters 10, 15, and 17 in the coculture and monoculture of *P. ostreatus* under optimal culture conditions were compared by RT-qPCR analysis. As shown in Figure 10a, the transcriptional levels of the genes encoding putative terpenoid synthase (KDQ25270), farnesyl-diphosphate farnesyltransferase (KDQ25271), and oxidase (KDQ25268) in clusters 10 under the optimal coculture conditions were found to be 13.6-fold, 261.5-fold, and 106.3-fold higher than those in the monoculture, respectively. These results were consistent with the increased titers of compounds **1** and **2** and further supported the speculation that compounds **1** and **2** were biosynthesized by cluster 10. Moreover, the transcriptional levels of genes encoding putative terpenoid synthase (KDQ23218) or oxidases (KDQ23216, KDQ23217, and KDQ23219) from cluster 17 were 4.5-fold, 1.5-fold, 11.1-fold, and 15.9-fold higher than those in the monoculture (Figure 10b), while the transcriptional levels of genes encoding putative terpenoid synthase (KDQ24004) or oxidases (including KDQ24003, KDQ24005, KDQ24006, etc.) from cluster 15 did not show obvious upregulation (Figure S9). These results suggested that cluster 17 is likely involved in the synthesis of compounds **3**−**5**. Protein BLAST analysis indicated that the putative terpenoid synthase (KDQ23218) had low sequence homology (the identities were less than 40%) among the protein database of basidiomycetes. This enzyme function will be studied in the future.

The biosynthetic pathways for compounds **1**−**5** were eventually proposed based on analysis of the structural features, gene functions, and RT-qPCR data. As shown in Scheme 1, GPP and FPP were likely catalyzed by putative farnesyl-diphosphate farnesyltransferase (KDQ25271) to form the unusual C_{25} precursor, which underwent further epoxidation catalyzed by putative squalene epoxidase (KDQ25268), followed by epoxide opening, loss of OH^-, cyclization, and hydroxylation to form compounds **1** and **2**, successively. Alternatively, if an intermediate **a** underwent cyclization and hydroxylation, it could also form compound **2**. On the other hand, we speculated that FPP could lose OPP^- and H^+ under the catalysis of putative terpenoid synthase (KDQ23218) before undergoing cyclization, oxidation, epoxidation, and epoxide opening under the catalysis of putative oxidase (KDQ23216 and KDQ23219), cytochrome P450 (KDQ23217), and a common epoxide hydrolase outside the cluster to form compounds **3**−**5**.

https://doi.org/10.1021/acs.jafc.3c03276
J. Agric. Food Chem. 2023, 71, 11110−11123

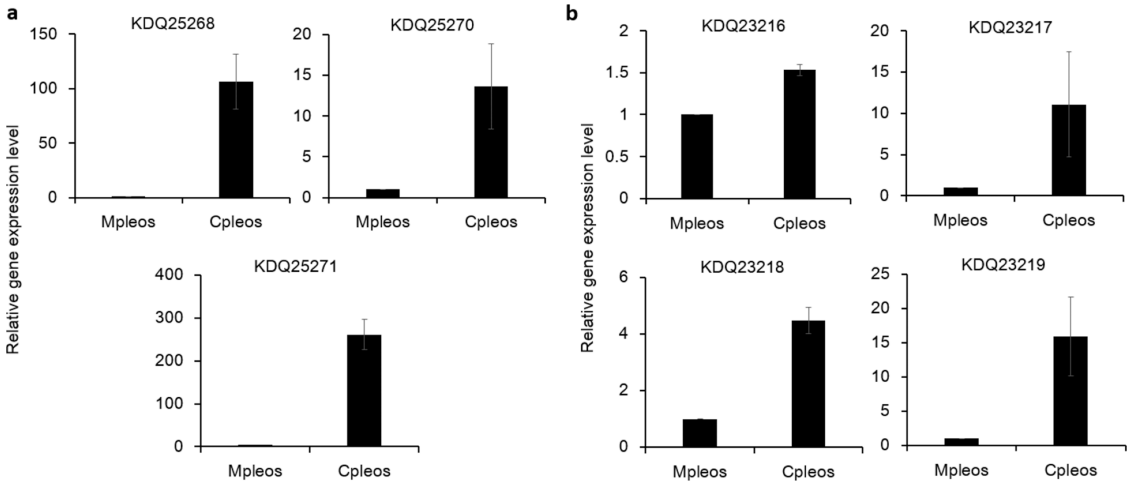

Figure 10. Comparison of the transcriptional level of gene clusters 10 (a) and 17 (b) in monoculture (Mpleos) and coculture (CPleos) of *P. ostreatus* under optimal culture conditions. The average level in monoculture was set to 1. Bars depict the means ± SD of three independent biological replicates.

Scheme 1. Hypothetical Biosynthetic Pathways for Compounds 1−5

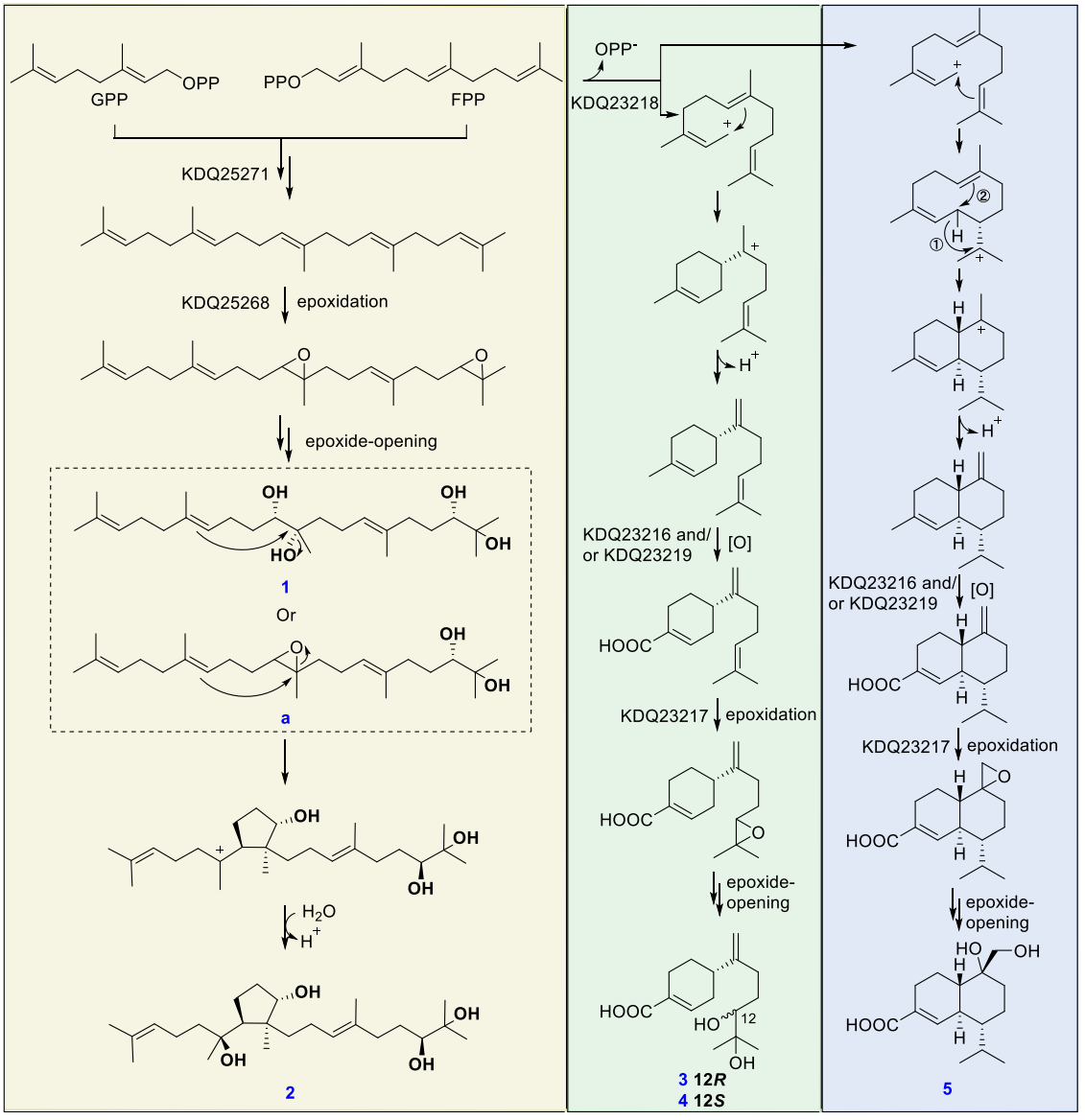

https://doi.org/10.1021/acs.jafc.3c03276
J. Agric. Food Chem. 2023, 71, 11110−11123

In summary, guided by genome mining analysis, we optimized coculture conditions using a single-factor test and BBD based on the OSMAC strategy. Furthermore, we carried out an in-depth examination of the optimized cocultivation system. As a result, the titers of novel antifungal terpenoids (**PA**−**PC**) were highly increased, and five new terpenoids with different degrees of antimicrobial activity, postredienes D−H (**1**−**5**), were discovered. Among these new compounds, compound **2** represented a novel skeleton that possesses a five-membered ring at C-7. The absolute configurations of **1**−**5** were determined in detail, possible gene clusters for synthesizing **1**−**5** were deduced by RT-qPCR, and relevant pathways were elucidated. The current work provides new insights into the study of terpenoid biosynthesis in *P. ostreatus* and other basidiomycetes.

■ ASSOCIATED CONTENT

Supporting Information

The Supporting Information is available free of charge at https://pubs.acs.org/doi/10.1021/acs.jafc.3c03276.

HRESIMS and 1D and 2D NMR spectra of compounds **1**−**5**, **A1**, **A2**, **1a**, **3′**, **3′a**, **3′b**, **4′**, **4′a**, and **4′b** (Figures S10−S67); structures of previously reported terpenoids from *P. ostreatus*; primers used for real-time RT-qPCR; information about clusters 10, 15, and 17; details for coculture optimization and computational calculation; and UPLC-MS analysis of the 14th day fermentation broth extracts from the monoculture of *P. ostreatus* SY10 and *T. robiniophila* SY636, as well as from the coculture of *P. ostreatus* SY10 with *T. robiniophila* SY636 (PDF)

■ AUTHOR INFORMATION

Corresponding Authors

Guihong Yu − *School of Life Sciences, Shandong Province Key Laboratory of Applied Mycology, and Qingdao International Center on Microbes Utilizing Biogas, Qingdao Agricultural University, Qingdao, Shandong Province 266109, People's Republic of China*; orcid.org/0000-0003-1900-0548; Email: Yuguihong1990@126.com

Song Yang − *School of Life Sciences, Shandong Province Key Laboratory of Applied Mycology, and Qingdao International Center on Microbes Utilizing Biogas, Qingdao Agricultural University, Qingdao, Shandong Province 266109, People's Republic of China*; orcid.org/0000-0002-4022-3941; Email: yangsong1209@163.com

Authors

Xiaoxuan Ge − *School of Life Sciences, Shandong Province Key Laboratory of Applied Mycology, and Qingdao International Center on Microbes Utilizing Biogas, Qingdao Agricultural University, Qingdao, Shandong Province 266109, People's Republic of China*

Yu Wang − *School of Life Sciences, Shandong Province Key Laboratory of Applied Mycology, and Qingdao International Center on Microbes Utilizing Biogas, Qingdao Agricultural University, Qingdao, Shandong Province 266109, People's Republic of China*

Xuhua Mo − *School of Life Sciences, Shandong Province Key Laboratory of Applied Mycology, and Qingdao International Center on Microbes Utilizing Biogas, Qingdao Agricultural University, Qingdao, Shandong Province 266109, People's Republic of China*; orcid.org/0000-0001-8515-3732

Hao Yu − *School of Life Sciences, Shandong Province Key Laboratory of Applied Mycology, and Qingdao International Center on Microbes Utilizing Biogas, Qingdao Agricultural University, Qingdao, Shandong Province 266109, People's Republic of China*

Lingling Tan − *School of Life Sciences, Shandong Province Key Laboratory of Applied Mycology, and Qingdao International Center on Microbes Utilizing Biogas, Qingdao Agricultural University, Qingdao, Shandong Province 266109, People's Republic of China*

Complete contact information is available at: https://pubs.acs.org/10.1021/acs.jafc.3c03276

Author Contributions

†G.Y., X.G., and Y.W. contributed equally.

Funding

This work was financially supported by the Shandong Provincial Key Research and Development Plan (2021ZDSYS28), the Natural Science Foundation of Shandong Province, China (ZR2020MC008 and ZR2021MC074), the High-level Talents Research Fund of Qingdao Agricultural University (Grants 665/1120034), and the National Natural Science Foundation of China (41806167).

Notes

The authors declare no competing financial interest.

■ REFERENCES

(1) Birch, A. J.; Holzapfel, C. W.; Rickards, R. W. The structure and some aspects of the biosynthesis of pleuromutilin. *Tetrahedron* **1966**, *22*, 359−387.

(2) Schobert, R.; Knauer, S.; Seibt, S.; Biersack, B. Anticancer active illudins: recent developments of a potent alkylating compound class. *Curr. Med. Chem.* **2011**, *18*, 790−807.

(3) Lesa, K. N.; Khandaker, M. U.; Mohammad Rashed Iqbal, F.; Sharma, R.; Islam, F.; Mitra, S.; Emran, T. B. Nutritional value, medicinal importance, and health-promoting effects of dietary mushroom (*Pleurotus ostreatus*). *J. Food Quality* **2022**, *2022*, No. 2454180.

(4) Pellegrino, R. M.; Blasi, F.; Angelini, P.; Ianni, F.; Alabed, H. B. R.; Emiliani, C.; Venanzoni, R.; Cossignani, L. LC/MS Q-TOF metabolomic investigation of amino acids and dipeptides in *Pleurotus ostreatus* grown on different substrates. *J. Agric. Food Chem.* **2022**, *70*, 10371−10382.

(5) Zhu, L.; Han, X.; Cui, X.; Li, S.; Qiao, L.; Chen, R. Two new alkaloids from *Pleurotus ostreatus* (Jacq.:Pers.) Roll. *Rec. Nat. Prod.* **2020**, *14*, 319−325.

(6) Shen, X.; Mo, X.; Zhu, L.; Tan, L.; Du, F.; Wang, Q.; Zhou, Y.; Yuan, X.; Qiao, B.; Yang, S. Unusual and highly bioactive sesterterpenes synthesized by *Pleurotus ostreatus* during coculture with *Trametes robiniophila* Murr. *Appl. Environ. Microbiol.* **2019**, *85*, No. e00293-19.

(7) Ge, X.; Wang, Y.; Sun, C.; Zhang, Z.; Song, L.; Tan, L.; Li, D.; Yang, S.; Yu, G. Secondary metabolites produced by coculture of *Pleurotus ostreatus* SY10 and *Pleurotus eryngii* SY302. *Chem. Biodiversity* **2022**, *19*, No. e202100832.

(8) Annang, F.; Pérez-Victoria, I.; Appiah, T.; Pérez-Moreno, G.; Domingo, E.; Martín, J.; Mackenzie, T.; Ruiz-Pérez, L.; González-Pacanowska, D.; Genilloud, O.; Vicente, F.; Agyare, C.; Reyes, F. Antiprotozoan sesterterpenes and triterpenes isolated from two Ghanaian mushrooms. *Fitoterapia* **2018**, *127*, 341−348.

(9) Rupcic, Z.; Rascher, M.; Kanaki, S.; Köster, R. W.; Stadler, M.; Wittstein, K. Two new cyathane diterpenoids from mycelial cultures of the medicinal mushroom *Hericium erinaceus* and the rare species, *Hericium flagellum*. *Int. J. Mol. Sci.* **2018**, *19*, 740.

(10) Friedman, M. Chemistry, nutrition, and health-promoting properties of *Hericium erinaceus* (Lion's Mane) mushroom fruiting bodies and mycelia and their bioactive compounds. *J. Agric. Food Chem.* **2015**, *63*, 7108−7123.
(11) Wang, K.; Bao, L.; Qi, Q.; Zhao, F.; Ma, K.; Pei, Y.; Liu, H. Erinacerins C-L, isoindolin-1-ones with α-glucosidase inhibitory activity from cultures of the medicinal mushroom *Hericium erinaceus*. *J. Nat. Prod.* **2015**, *78*, 146−154.
(12) Alberti, F.; Khairudin, K.; Venegas, E. R.; Davies, J. A.; Hayes, P. M.; Willis, C. L.; Bailey, A. M.; Foster, G. D. Heterologous expression reveals the biosynthesis of the antibiotic pleuromutilin and generates bioactive semi-synthetic derivatives. *Nat. Commun.* **2017**, *8*, 1831.
(13) Mapook, A.; Hyde, K. D.; Hassan, K.; Kemkuignou, B. M.; Čmoková, A.; Surup, F.; Kuhnert, E.; Paomephan, P.; Cheng, T.; de Hoog, S.; Song, Y.; Jayawardena, R. S.; Al-Hatmi, A. M. S.; Mahmoudi, T.; Ponts, N.; Studt-Reinhold, L.; Richard-Forget, F.; Chethana, K. W. T.; Harishchandra, D. L.; Mortimer, P. E.; Li, H.; Lumyong, S.; Aiduang, W.; Kumla, J.; Suwannarach, N.; Bhunjun, C. S.; Yu, F.; Zhao, Q.; Schaefer, D.; Stadler, M. Ten decadal advances in fungal biology leading towards human well-being. *Fungal Divers.* **2022**, *116*, 547−614.
(14) Gressler, M.; Löhr, N. A.; Schäfer, T.; Lawrinowitz, S.; Seibold, P. S.; Hoffmeister, D. Mind the mushroom: natural product biosynthetic genes and enzymes of Basidiomycota. *Nat. Prod. Rep.* **2021**, *38*, 702−722.
(15) Scherlach, K.; Hertweck, C. Triggering cryptic natural product biosynthesis in microorganisms. *Org. Biomol. Chem.* **2009**, *7*, 1753−1760.
(16) Zhang, T.; Cai, G.; Rong, X.; Wang, Y.; Gong, K.; Liu, W.; Wang, L.; Pang, X.; Yu, L. A combination of genome mining with an OSMAC approach facilitates the discovery of and contributions to the biosynthesis of melleolides from the basidiomycete *Armillaria tabescens*. *J. Agric. Food Chem.* **2022**, *70*, 12430−12441.
(17) Yu, J.; Han, H.; Zhang, X.; Ma, C.; Sun, C.; Che, Q.; Gu, Q.; Zhu, T.; Zhang, G.; Li, D. Discovery of two new sorbicillinoids by overexpression of the global regulator LaeA in a marine-derived fungus *Penicillium dipodomyis* YJ-11. *Mar. Drugs* **2019**, *17*, 446.
(18) Shwab, E. K.; Bok, J. W.; Tribus, M.; Galehr, J.; Graessle, S.; Keller, N. P. Histone deacetylase activity regulates chemical diversity in *Aspergillus*. *Eukaryotic Cell* **2007**, *6*, 1656−1664.
(19) Sugano, S. S.; Suzuki, H.; Shimokita, E.; Chiba, H.; Noji, S.; Osakabe, Y.; Osakabe, K. Genome editing in the mushroom-forming basidiomycete *Coprinopsis cinerea*, optimized by a high-throughput transformation system. *Sci. Rep.* **2017**, *7*, 1260.
(20) Qin, H.; Xiao, H.; Zou, G.; Zhou, Z.; Zhong, J. CRISPR-Cas9 assisted gene disruption in the higher fungus *Ganoderma* species. *Process Biochem.* **2017**, *56*, 57−61.
(21) Barh, A.; Sharma, V. P.; Annepu, S. K.; Kamal, S.; Sharma, S.; Bhatt, P. Genetic improvement in Pleurotus (oyster mushroom): a review. *3 Biotech* **2019**, *9*, 322.
(22) Bode, H. B.; Bethe, B.; Hofs, R.; Zeeck, A. Big effects from small changes: possible ways to explore nature's chemical diversity. *ChemBioChem* **2002**, *3*, 619−627.
(23) Yu, G.; Sun, Y.; Han, H.; Yan, X.; Wang, Y.; Ge, X.; Qiao, B.; Tan, L. Coculture, an efficient biotechnology for mining the biosynthesis potential of macrofungi via interspecies interactions. *Front. Microbiol.* **2021**, *12*, No. 663924.
(24) Riley, R.; Salamov, A. A.; Brown, D. W.; Nagy, L. G.; Floudas, D.; Held, B. W.; Levasseur, A.; Lombard, V.; Morin, E.; Otillar, R.; Lindquist, E. A.; Sun, H.; LaButti, K. M.; Schmutz, J.; Jabbour, D.; Luo, H.; Baker, S. E.; Pisabarro, A. G.; Walton, J. D.; Blanchette, R. A.; Henrissat, B.; Martin, F.; Cullen, D.; Hibbett, D. S.; Grigoriev, I. V. Extensive sampling of basidiomycete genomes demonstrates inadequacy of the white-rot/brown-rot paradigm for wood decay fungi. *Proc. Natl. Acad. Sci. U. S. A.* **2014**, *111*, 9923−9928.
(25) Othman, A. M.; Mahmoud, M.; Abdelraof, M.; Abdel Karim, G. S. A.; Elsayed, A. M. Enhancement of laccase production from a newly isolated *Trichoderma harzianum* S7113 using submerged fermentation: optimization of production medium via central composite design and its application for hydroquinone degradation. *Int. J. Biol. Macromol.* **2021**, *192*, 219−231.
(26) Wu, Z. Mixed fermentation of Aspergillus niger and Candida shehatae to produce bioethanol with ionic-liquid-pretreated bagasse. *3 Biotech* **2019**, *9*, 41.
(27) Seong, H.-J.; Im, A. E.; Kim, H.; Park, N.; Yang, K.-Y.; Kim, D.; Nam, S.-H. Production of prunin and naringenin by using naringinase from *Aspergillus oryzae* NYO-2 and their neuroprotective properties and debitterization. *J. Agric. Food Chem.* **2023**, *71*, 1655−1666.
(28) He, X.; Zhang, Z.; Chen, Y.; Che, Q.; Zhu, T.; Gu, Q.; Li, D. Varitatin A, a highly modified fatty acid amide from *Penicillium variabile* cultured with a DNA methyltransferase inhibitor. *J. Nat. Prod.* **2015**, *78*, 2841−2845.
(29) Grimblat, N.; Zanardi, M. M.; Sarotti, A. M. Beyond DP4: an improved probability for the stereochemical assignment of isomeric compounds using quantum chemical calculations of NMR shifts. *J. Org. Chem.* **2015**, *80*, 12526−12534.
(30) Li, J.; Chen, M.; Hao, X.; Li, S.; Li, F.; Yu, L.; Xiao, C.; Gan, M. Structural revision and absolute configuration of burnettramic acid A. *Org. Lett.* **2020**, *22*, 98−101.
(31) Yu, G.; Wu, G.; Sun, Z.; Zhang, X.; Che, Q.; Gu, Q.; Zhu, T.; Li, D.; Zhang, G. Cytotoxic tetrahydroxanthone dimers from the mangrove-associated fungus *Aspergillus versicolor* HDN1009. *Mar. Drugs* **2018**, *16*, 335.
(32) Livak, K. J.; Schmittgen, T. D. Analysis of relative gene expression data using real-time quantitative PCR and the 2(−delta delta C(T)) method. *Methods* **2001**, *25*, 402−408.
(33) Sun, T.; Wang, R.; Sun, D.; Li, S.; Xu, H.; Qiu, Y.; Lei, P.; Sun, L.; Xu, X.; Zhu, Y. High-efficiency production of *Tremella aurantialba* polysaccharide through basidiospore fermentation. *Bioresour. Technol.* **2020**, *318*, No. 124268.
(34) Chaverra-Muñoz, L.; Briem, T.; Hüttel, S. Optimization of the production process for the anticancer lead compound illudin M: improving titers in shake-flasks. *Microb. Cell Fact.* **2022**, *21*, 98.
(35) Wang, X.; Ding, Z.; Liu, G.; Yang, H.; Zhou, G. Improved production and antitumor properties of triterpene acids from submerged culture of *Ganoderma lingzhi*. *Molecules* **2016**, *21*, 1395.
(36) Wei, Z.; Duan, Y.; Qian, Y.; Guo, X.; Li, Y.; Jin, S.; Zhou, Z.; Shan, S.; Wang, C.; Chen, X.; Zheng, Y.; Zhong, J. Screening of *Ganoderma* strains with high polysaccharides and ganoderic acid contents and optimization of the fermentation medium by statistical methods. *Bioprocess Biosyst. Eng.* **2014**, *37*, 1789−1797.
(37) Liu, G.; Ren, G.; Wang, X.; Zhao, Y. Statistical optimization of the key medium components by response surface methodology to promote ganoderic acid formation by medicinal mushroom *Ganoderma sinense* in submerged culture. *J. Med. Plants Res.* **2011**, *5*, 425−431.
(38) Wang, S.; Wu, S.; He, Q.; Li, Z.; Zhang, X.; Sun, Y.; Zhu, C.; He, H.; Jiang, S.; Bao, R. Application of response surface optimization in production of ganoderic acid by submerged fermentation of *Ganoderma lucidum*. CN104212867, 2014.
(39) Yu, G.; Sun, P.; Aierken, R.; Sun, C.; Zhang, Z.; Che, Q.; Zhang, G.; Zhu, T.; Gu, Q.; Li, M.; Li, D. Linear polyketides produced by co-culture of *Penicillium crustosum* and *Penicillium fellutanum*. *Mar. Life Sci. Technol.* **2022**, *4*, 237−244.
(40) Seco, J. M.; Quiñoá, E.; Riguera, R. The assignment of absolute configuration by NMR. *Chem. Rev.* **2004**, *104*, 17−118.
(41) Raju, R.; Gromyko, O.; Fedorenko, V.; Luzhetskyy, A.; Plaza, A.; Müller, R. Juniperolide A: a new polyketide isolated from a terrestrial actinomycete, Streptomyces sp. *Org. Lett.* **2012**, *14*, 5860−5863.
(42) Hashidoko, Y.; Urashima, M. Efficient preparation of browning-free glandular trichome tissues from the surface of leaves of Rosa rugosa Thunb. *Plant Cell Physiol.* **1995**, *36*, 127−132.
(43) Cheng, T.; Chepkirui, C.; Decock, C.; Matasyoh, J. C.; Stadler, M. Sesquiterpenes from an eastern African medicinal mushroom belonging to the genus *Sanghuangporus*. *J. Nat. Prod.* **2019**, *82*, 1283−1291.

(44) Yu, G.; Zhou, G.; Zhu, M.; Wang, W.; Zhu, T.; Gu, Q.; Li, D. Neosartoryadins A and B, fumiquinazoline alkaloids from a mangrove-derived fungus *Neosartorya udagawae* HDN13-313. *Org. Lett.* **2016**, *18*, 244−247.
(45) Liu, S.; Zhao, Y.; Heering, C.; Janiak, C.; Müller, W. E. G.; Akoné, S. H.; Liu, Z.; Proksch, P. Sesquiterpenoids from the endophytic fungus *Rhinocladiella similis*. *J. Nat. Prod.* **2019**, *82*, 1055−1062.
(46) Yin, R.; Zhao, Z.; Ji, X.; Dong, Z.; Li, Z.; Feng, T.; Liu, J. Steroids and sesquiterpenes from cultures of the fungus *Phellinus igniarius*. *Nat. Prod. Bioprospect.* **2015**, *5*, 17−22.
(47) Mitsuhashi, T.; Abe, I. Chimeric terpene synthases possessing both terpene cyclization and prenyltransfer activities. *ChemBioChem* **2018**, *19*, 1106−1114.
(48) Stadler, M.; Baumgartner, M.; Grothe, T.; Mühlbauer, A.; Seip, S.; Wollweber, H. Concentricol, a taxonomically significant triterpenoid from *Daldinia concentrica*. *Phytochemistry* **2001**, *56*, 787−793.
(49) Chepkirui, C.; Yuyama, K. T.; Wanga, L. A.; Decock, C.; Matasyoh, J. C.; Abraham, W.-R.; Stadler, M. Microporenic acids A−G, biofilm Inhibitors, and antimicrobial agents from the Basidiomycete *Microporus* Species. *J. Nat. Prod.* **2018**, *81*, 778−784.

https://doi.org/10.1021/acs.jafc.3c03276
J. Agric. Food Chem. 2023, 71, 11110−11123